9th AUSTRALASIAN
FLUID MECHANICS CONFERENCE,
AUCKLAND, 8-12 DECEMBER 1986

Mean and Fluctuating Velocity in a Low Reynolds Number Boundary Layer

P. V. LANSPEARY

Department of Mechanical Engineering, University of Adelaide, Australia.

ABSTRACT

One of the difficulties in measuring small scale phenomena in a turbulent boundary layer is that the probe size is large compared with the length scales of the phenomena. In order to ameliorate this problem, an attempt has been made to increase the ν/u_τ length scale to between 0.03 and 0.24 mm by reducing free stream velocity by about an order of magnitude. Although this has been done successfully, the resulting momentum thickness based Reynolds number Re_θ is always less than 6000, and it is necessary to establish that the boundary layer is genuinely turbulent, is in equilibrium and is two dimensional. Coles (1962) has determined that a normal boundary layer can be recognized by examining both the turbulent wake strength of the mean profile and the momentum balance of the boundary layer. Friction coefficients, profiles of mean air speed, turbulence level, skewness and flatness, probability density, power spectral densities and autocorrelations of the streamwise velocity have also been examined for signs of irregularity or periodicity in the signal and compared with published data. It was discovered that, as stated by Coles (1962), it is by no means as easy to generate a proper turbulent boundary layer as is commonly supposed.

EXPERIMENTAL ARRANGEMENT

Wind Tunnel

The 0.23m square test section, 25:1 contraction low-noise wind tunnel used by Thomas (1977) has been modified to operate at much lower flow rates. The flow rate induced in the open-circuit wind tunnel is controlled by a variable-throat-area sonic choke which also stops noise from the drive compressor reaching the test section. The sliding centre-body of the choke has been replaced by another of larger diameter both to reduce the flow rate and to increase the maximum/minimum speed ratio. A second choked by-pass flow from atmosphere ensures stable operation of the compressor. The boundary layer being studied is developed on the roof of the test section. A 500mm long extension was added to the upstream end of the working section to increase development length and accommodate a boundary layer trip. The working section is constructed from rigid, heavy aluminium section. A flexible stainless steel floor allows accurate setting of the streamwise pressure gradient. For the present experiments the pressure gradient was zero at a speed of about 4.5 m/s, was slightly positive at higher speeds and was negative at lower speeds. There are fifteen 151 mm diameter instrumentation ports in the roof of the working section.

Instrumentation and Data Acquisition System

The relationship between low dynamic pressure in the wind tunnel working section and the higher dynamic pressure just upstream of the variable-area sonic choke has been determined over the full operating speed range of the wind tunnel. From this, free stream speed at any port in the working section can be determined by a pitot-static tube and MKS Baratron transducer, so avoiding the problems of measuring dynamic pressures of the order of 1 Pa.

The centre of the data acquisition system is an SBC100M microcomputer which controls 2 A/D converters and a large "Quasi Disk" RAM, a probe traverse mechanism and data transmission to a PDP11/34 mini-computer. The PDP11/34, which runs under the multiuser UNIX.L7 operating system, acts as an intelligent controller of the SBC100M. The data acquisition program for the PDP11/34 is extremely flexible and automates the data collection procedure.

The anemometer probe is a single 5μm diameter tungsten hot wire operated at constant temperature with an overheat of 0.5. For some experiments 0.6μmx0.2mm long Pt/Rh wires were used with a lower overheat.

Wall Proximity Effect on Velocity Measurements

A preliminary experiment was conducted to find an acceptable probe configuration, in particular, to minimize the wall proximity effect due primarily to heat transfer to the wall. Decreasing wire diameter and overheat ratio both reduced wall proximity effects but there were deleterious side effects such as increased drift, difficulty in manufacture and fragility, together with poorer frequency response and sensitivity. For free stream air speeds of less than 10 m/s, wall insulation by a 0.5mm thick sheet of high impact polystyrene only reduces the wall proximity effect by about 30% from values given by Krishnamoorthy (1985), but this measure was adopted because no deleterious side-effects were observed.

Details of probe geometry can significantly influence wall proximity effect. In the present work the prongs were kept well away from the heated part of the wire by bending the wire into the shape of a flat bottomed U before soldering it to the prongs. The final prong angle of incidence is about 3 degrees. The length of the active part of the wire is 1.3 mm, which in non-dimensional terms is $11<\ell^+<36$.

C.T.A. Bridge and Instrumentation Amplifier

The CTA bridges to operate the wires were designed and built in accordance with the recommendations of Perry & Morrison (1971). The instability encountered when operating 0.6μm diameter wires can be solved by inserting a 100pF to 500pF compensation capacitor in parallel with the overheat resistor. The instrumentation amplifiers used to match the CTA bridge output to the A/D converter each have a 6 pole low pass Bessel filter with a 3dB cut-off frequency of 18kHz (which is at least three times the highest signal frequencies). The filters have constant group delay.

Calibration of Hot Wires

Experience has demonstrated that hot wires must be calibrated over the whole range of expected mean velocities. It is difficult to measure air speeds of less than 1.5m/s accurately with a pitot tube. Lower air speeds were measured by using a separate hot wire to detect the frequency of laminar vortex shedding from a cylinder placed about 0.3m downstream of the hot wire being calibrated. The air speed was calculated by using Liepmann's formula. A law of the form $E_0^2=a+bU^n+cU^{2n}$ was fitted to the data of each calibration, with the exponent n being selected to

Fig 1. Inner Region - Mean Velocity

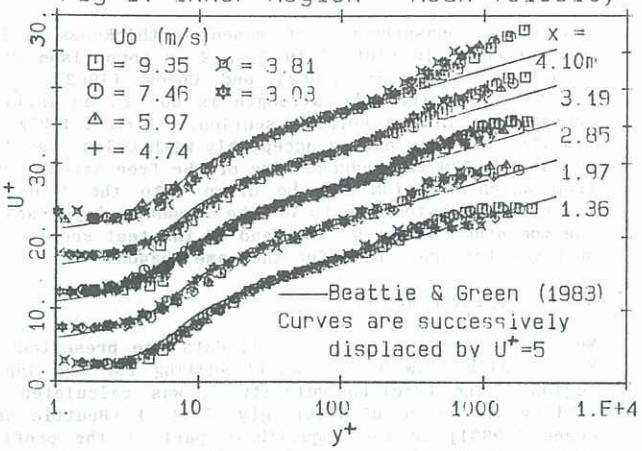

Fig 1. Outer Region - Mean Velocity

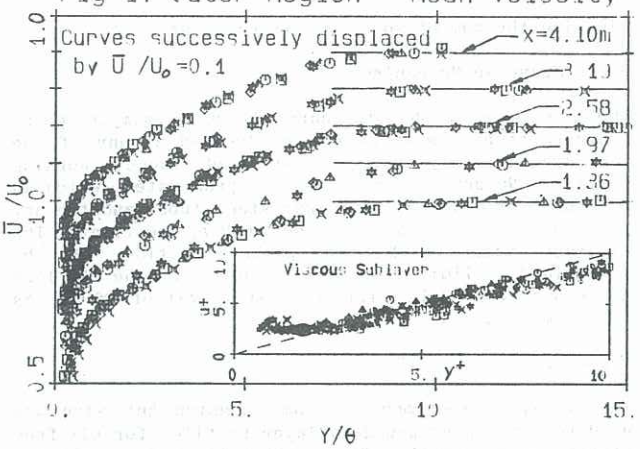

Fig 2. Inner Region - RMS Velocity

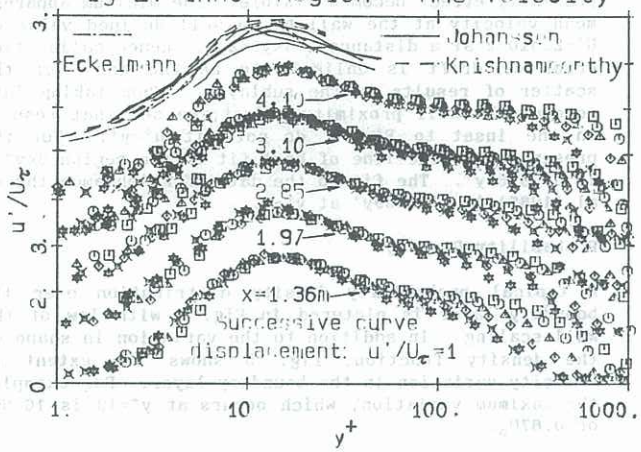

Outer Region -Local Turbulence Level

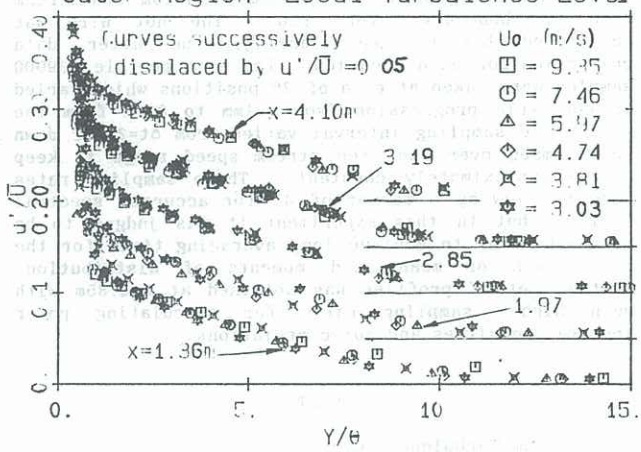

Fig 3. Inner region - Skewness

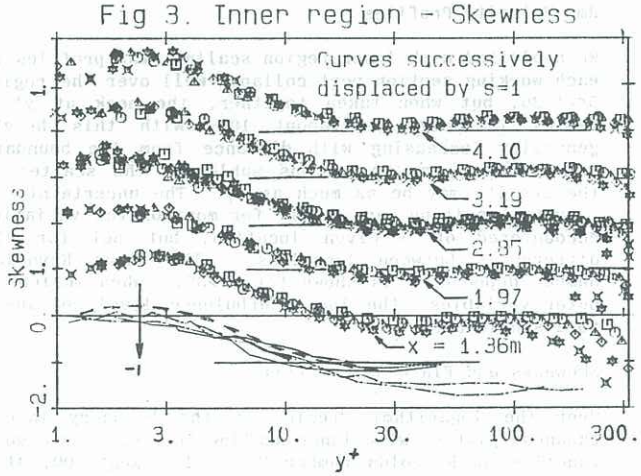

Fig 3. Outer Region - Skewness

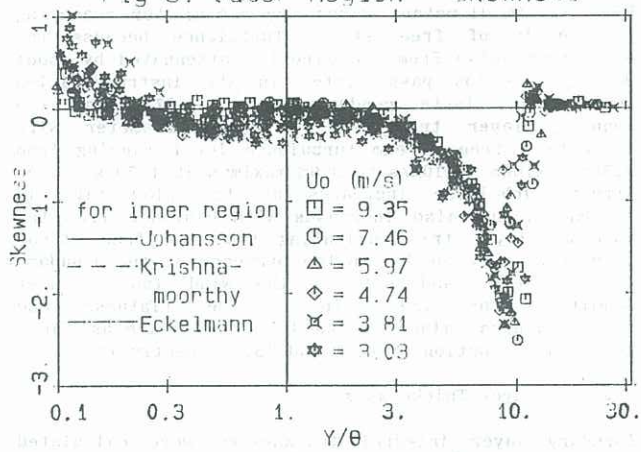

Fig 4. Inner Region - Flatness

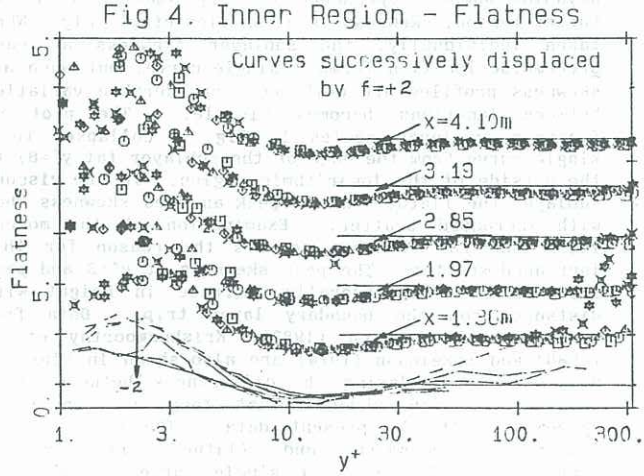

Fig 4. Outer Region - Flatness

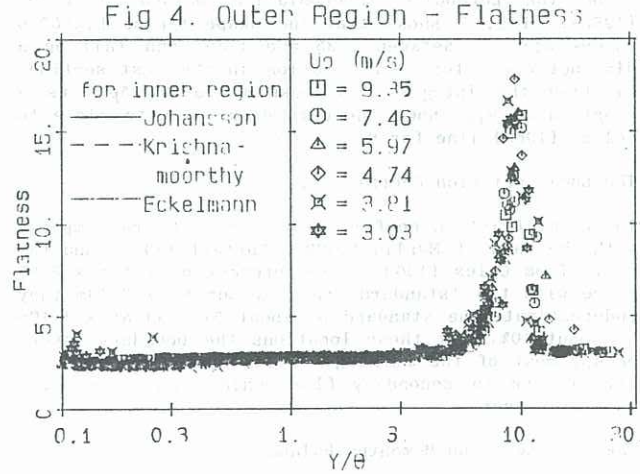

minimize the sum of squared fitting error.

Probe Traverse Mechanism

The hot wire probe is carried in a simple probe traverse mechanism which can be located at any of the instrumentation plugs in the wind tunnel working section. No device apart from the probe stem, which is made of 3 mm diameter stainless steel tube, and the hot wire itself intrudes into the working section. The accuracy with which the probe position can be determined is limited by the resolution of the DAS 1128 A/D converter which, for a total travel of 80 mm, is 0.025 mm.

Procedure

In the main experiment, a 5μm tungsten hot wire was used for obtaining boundary layer profiles for six free stream speeds ranging from 9.3m/s to 3.0m/s, and for five locations ranging from 1.36m to 4.10m downstream from the boundary layer trip. The hot wire was calibrated before, once during, and after data collection for each location. For each profile, 39900 samples were taken at each of 26 positions which varied in geometric progression from 0.1mm to 80mm from the wall. The sampling interval varied from Δt=2mSec down to 0.48mSec over the free stream speed range to keep $U_o\Delta t/\theta$ approximately constant. These sampling rates were too low by a factor of 4, for accurate spectral analysis but in this experiment it was judged to be more important to achieve long averaging times for the calculation of means and moments of distribution. Another set of profiles was obtained at x=2.85m with much higher sampling rates for calculating power spectral densities and autocorrelations.

RESULTS

Free Stream Turbulence Level

Fine (0.6μm diameter) wires are useful for measuring low levels of free stream turbulence because the electronic noise from the wire is attenuated by about 90% by the low pass filter in the instrumentation amplifier. Tests conducted at x=1.97m from the boundary layer trip using a 0.6μm diameter wire indicate a free stream turbulence level ranging from 0.25% maximum at 10m/s to 0.9% maximum at 1.5m/s. Free stream turbulence increases as the flow rate is decreased, and also increases with distance from the boundary layer trip indicating that the free stream turbulence must be due to the presence of the boundary layer itself, and not to the wind tunnel inlet conditions or the trip. The flatness and super-flatness values in the free stream are as for a normal distribution (i.e. 3 and 15) respectively.

Boundary Layer Thicknesses

Boundary layer integral thicknesses were calculated using the parabolic interpolation method of Coles (1968). Fig. 7 shows that the shape factor $H_{12}=\delta^*/\theta$ values all lie between 1.35 and 1.45, and fall on a distinct curve for each location in the test section. Plotting the integral thickness ratio $H_{32}=\delta_E/\theta$ as a function of H_{12} shows the data grouped quite close to Coles' (1968) line for Re_{δ^*}=1000.

The Local Friction Coefficient

The Local Friction coefficients in Fig. 8 are compared with the data of Murlis (1982), Purtell (1981) and the curve from Coles (1968). The present data for x≤2.85 agree with the 'standard' results but at x=3.19m they underestimate the standard by about 5%, and at x=4.10m by about 10%. At these locations the boundary layers occupy most of the working section area (80% and 87%) giving rise to secondary flows which contaminate the boundary layer.

Wake Strength and Momentum Balance

The erratic momentum balance results (Fig.10) are due to scatter in measurements of momentum thickness. The wake strength is plotted in Fig. 9 in comparison with results from Murlis (1982) and Coles (1962). At x=1.36m the small wake strength is due to an initial contraction in the working section. From x=1.97m to x=3.19m, the data agrees acceptably with Coles' result, but at x=4.10m the reduced size of the free stream zone from which momentum can be drawn into the boundary layer, accelerates growth of the boundary layer wake. The momentum balance at this end of the test section is much greater than unity for the same reason.

Mean Velocity Profiles

Mean velocity profiles from all data are presented in Fig. 1 with "law of the wall" scaling for the inner region. The friction velocity U_τ was calculated by fitting the curve $u^+=5.66(\log(y^+-5.4)+1)$ [Beattie and Green (1983)] to the logarithmic part of the profile data. At distances from the wall of $y^+<3$, the wall proximity effect becomes visible. The minimum apparent mean velocity at the wall has a well defined value of $U^+=2.4\pm0.2$ at a distance $1.4<y^+<2.1$. Hence calibration error or drift is unlikely to be the cause of the scatter of results in the sublayer. When taking into account the wall proximity effect, we see that results in the inset to Fig. 1 do not fit $u^+=y^+$. For the present data, the line of best fit in the region $3<y^+<7$ is $u^+=0.87y^+$. The fit to the data of Krishnamoorthy et al (1985) is $u^+=0.89y^+$ at $y^+=5$.

Probability Density

A typical probability density distribution over the boundary layer is pictured in Fig. 5 with law of the wall scaling. In addition to the variation in shape of the density function, Fig. 5 shows the extent of velocity variation in the boundary layer. For example, the maximum variation, which occurs at $y^+=13$ is $16.5u_\tau$ or $0.67U_o$.

Rms Velocity Profiles

When plotted with inner region scaling, the profiles at each working section port collapse well over the region $5<y^+<30$, but when taken together, the peak at $y^+=14$ varies in height by about 10%, with this height generally increasing with distance from the boundary layer trip. In the viscous sublayer, the scatter in the results may be as much as U_τ. The uncertainty in traverse position can account for most of the variation encountered of a given location, but not for the differences between locations. The usual Reynolds number dependence is shown for $y^+>30$. When scaled on outer variables the local turbulence level collapses to a single curve.

Skewness and Flatness Profiles

Over the logarithmic region of the boundary layer, skewness plotted with inner scaling in Fig. 3 is also a function of Reynolds number Re_θ. For $Re_\theta>2000$, this Reynolds number dependence is very small. Over the buffer region, skewness is a function of y^+ only. When taken individually, the sublayer skewness at each streamwise location forms a single curve, but when all skewness profiles are combined, considerable variation between locations becomes visible. The plot of flatness on inner scales in Fig. 4 collapses to a single curve from the edge of the sublayer (at $y^+=8$) to the outside of the logarithmic region. In the viscous sublayer the flatness has a peak as does skewness, but with increased scatter. Examination of the moment integrands for flatness reveals the reason for this increased scatter. The peak skewness at $y^+=3$ and peak flatness at $y^+=2$ generally increase in height with distance from the boundary layer trip. Data from Johanson and Afredson (1982), Krishnamoorthy et al (1985) and Eckelmann (1974) are also shown in Figs. 2, 3 and 4. Considering the differences between these results, we can observe that they are in broad agreement with the present data. The outer region scaling of skewness and flatness produces an approximate collapse to a single curve in the wake region of the boundary layer. There are insufficient

data and scatter of results is too great to determine whether the appropriate length scale is θ or δ^*. There is a well defined demarcation between the boundary layer and the free stream at $y/\theta=11$. Note that skewness is slightly positive at the edge of the free stream.

Higher Moments of Distribution

Super-skewness (5th moment) and super-flatness (6th moment) of the distribution have been calculated and have broadly the shapes of the skewness and flatness respectively. The main differences are that high values are accentuated, and the scatter in values obtained is much greater.

Autocorrelations and Power Spectral Densities

The best spectral density results were obtained by normalizing time scales with U_0/θ and the energy scale with U_τ^2. The power spectral densities and auto-correlations calculated from the high sampling rate data were unexceptional, and contained no signs of irregularity or periodicity.

CONCLUDING REMARKS

Results presented for the logarithmic region of the boundary layer are completely normal. The variability of moments of distribution in the sublayer might be due to secondary flows (which reduce the local friction coefficient) or local variations in pressure gradient. The calculation of momentum balance is sensitive to reduction of free stream width by the side-wall boundary layer. Wake strength is also sensitive to pressure gradients upstream of the probe.

REFERENCES

Beattie, D.R.H. & Green, W.J. (1983): A Simplified and Accurate Method of Describing Non-Turbulent transport of Momentum in Turbulent Flow Theory. Proc. Eighth Australasian Fluid Mechanics Conference. 10A.5-9 University of Newcastle.

Coles, D.E. (1962): A manual of Experimental Boundary Layer Practice for Low Speed Flow. Appendix A to NACA Report No. TR-403-PR.

Coles, D.E. and Hirst, E.A. (1968): The Young Person's Guide to the Data. AFOSR-IFP-Stanford Conference on Computation of Turbulent Boundary Layers.

Eckelmann, H. (1974): The Structure of the Viscous Sublayer and the Adjacent Wall Region in a Turbulent Channel Flow. Journal of FLuid Mechanics Vol. 65, pp 439-459.

Johanson, A.V. & Alfredson, AP.H. (1982): On the Structure of Turbulent Channel Flow. Journal of Fluid Mechanics Vol. 122 pp 295-314.

Krishnamoorthy, L.V., Wood, D.H., Chambers, A.J., Antonia R A. (1985): Effect of Wire Diameter and Overheat Ratio Near a Conducting Wall. Experiments in Fluids 3, 121-127.

Murlis, J., Tsai, H.M., & Bradshaw, P. (1982): The Structure of Turbulent Boundary Layers at Low Reynolds Numbers. Journal of Fluid Mechanics Vol. 122 pp 13-56.

Purtell, L.P., Klebanoff, P.S. and Buckley, F.T. (1981): Turbulent Boundary Layer at Low Reynolds Number. Physics of Fluids Vol 24(5) pp 802-811.

Perry, A.E. & Morrison, G.L. (1971): A Study of the Constant Temperature Hot Wire Anemometer. Journal of Fluid Mechanics, Vol 47 pp 577-599.

Thomas A S W. (1977): Organized Structures in the Turbulent Boundary Layer. Ph.D. Thesis, Dept. of Mech. Eng. University of Adelaide.

Fig 5. PDF of Streamwise Velocity

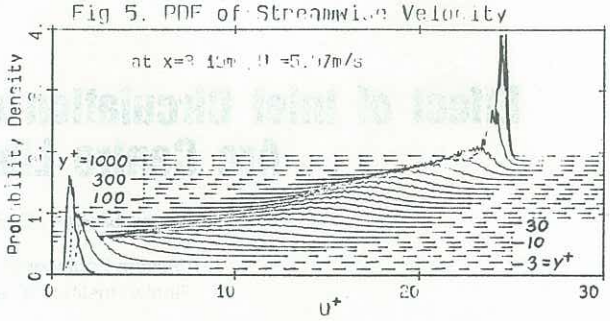

Fig 6. Integral thickness ratios

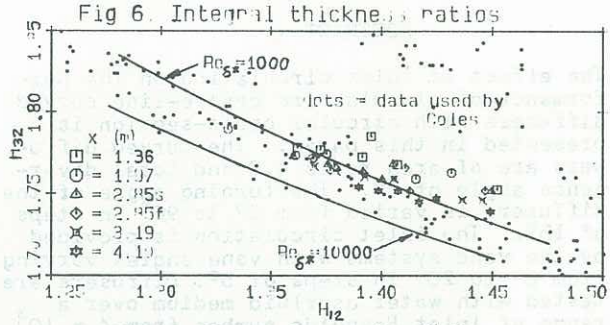

Fig 7. Shape factor $H_{12}=\delta^*/\theta$

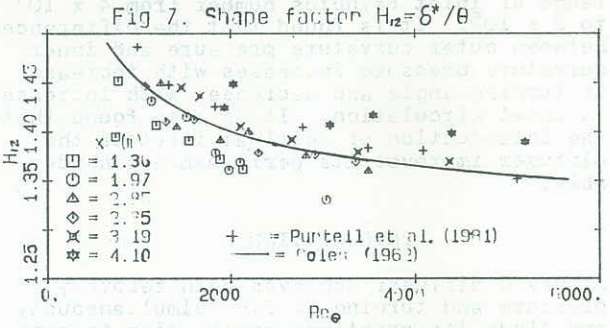

Fig 8. Local Friction Coefficient

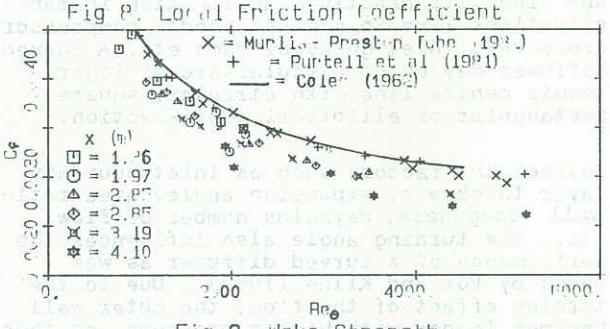

Fig 9. Wake Strength

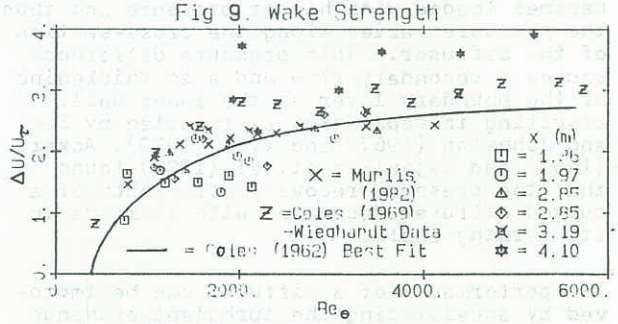

Fig 10. Momentum Balance